Published in final edited form as:
J Biomed Mater Res B Appl Biomater. 2007 April ; 81(1): 30–39.

Sensate Scaffolds Can Reliably Detect Joint Loading

C. L. Bliss, **J. A. Szivek**, **B. C. Tellis**, **D. S. Margolis**, **A. B. Schnepp**, and **J. T. Ruth**
Orthopedic Research Laboratory, Department of Surgery, University of Arizona, Tucson, Arizona 85724

Abstract

Treatment of cartilage defects is essential to the prevention of osteoarthritis. Scaffold-based cartilage tissue engineering shows promise as a viable technique to treat focal defects. Added functionality can be achieved by incorporating strain gauges into scaffolds, thereby providing a real-time diagnostic measurement of joint loading. Strain-gauged scaffolds were placed into the medial femoral condyles of 14 adult canine knees and benchtop tested. Loads between 75 and 130 N were applied to the stifle joints at 30°, 50°, and 70° of flexion. Strain-gauged scaffolds were able to reliably assess joint loading at all applied flexion angles and loads. Pressure sensitive films were used to determine joint surface pressures during loading and to assess the effect of scaffold placement on joint pressures. A comparison of peak pressures in control knees and joints with implanted scaffolds, as well as a comparison of pressures before and after scaffold placement, showed that strain-gauged scaffold implantation did not significantly alter joint pressures. Future studies could possibly use strain-gauged scaffolds to clinically establish normal joint loads and to determine loads that are damaging to both healthy and tissue-engineered cartilage. Strain-gauged scaffolds may significantly aid the development of a functional engineered cartilage tissue substitute as well as provide insight into the native environment of cartilage.

Keywords

sensors; articular cartilage; tissue engineering

INTRODUCTION

Articular cartilage has a poor healing response because it lacks resident pluripotent cells and is avascular. Failure to resolve tissue injury weakens the structural integrity of the cartilage, leading to progressive deterioration of surrounding cartilage. As such, even minor lesions can lead to wide-spread joint degeneration and osteoarthritis.[1] Development of surgical procedures to repair focal defects is critical to the maintenance of healthy joints. A number of techniques have been developed to aid the reparative process; however, all have notable limitations. Autologous tissue transplants[2–4] can cause donor site morbidity,[5,6] and autologous cell transplant procedures[7,8] often result in poor cell attachment, leading to incomplete healing[9–11] and fibro-cartilage tissue formation.

There has been a recent interest in the development of biodegradable scaffolds to support implantable tissues grown *in vitro*.[12] These scaffolds have been created from a wide variety of materials,[12–19] including polylactic acid, silk protein, polyester, and polybutylene terephthalate. The use of polymer scaffolds in tissue engineering offers many advantages. Nutrients and growth factors[20–24] can be incorporated into scaffold structures to continuously deliver necessary supplements to newly formed musculoskeletal tissues, encouraging rapid

Correspondence to: C. L. Bliss (e-mail: cbliss@u.arizona.edu).

development and integration into existing tissues. Scaffolds can be created in a variety of geometric configurations to allow implantation of engineered tissues that are tailored to fit an array of focal defect shapes.[25] Growing cartilage on scaffolds *in vitro* provides a more complete development of the tissue prior to implantation.[26,27] Bone readily grows into implantable scaffolds,[28–30] providing secure long-term attachment of engineered tissues to the surrounding tissues in the implant site. Additionally, osteoconductive coatings can be applied to scaffolds to accelerate bone ingrowth.[30,31]

To develop functional tissue-engineered cartilage, a thorough understanding of loads acting on cartilage is essential. By adding strain sensors to scaffolds used in tissue engineering, a complete *in vivo* tissue loading history can be recorded through real time monitoring of joint forces. Insights into cartilage mechanics, pluripotent cartilage pre-cursor cell triggers, and local material properties can be discovered from these measurements. Moreover, development of a technique that provides continuous *in vivo* measurements and data acquisition will make available clinically relevant diagnostic measurements during surgery and rehabilitation.[1,32] In addition, implanted sensors and data acquisition systems can be configured to generate warning signals in order to prevent joint overload.[33] This can help patients prevent damage to tissue-engineered cartilage during daily activities in the postsurgical healing period.

Adding sensors to a rapidly evolving scaffold design will also provide insight into the next essential step in the development of scaffolds and functional tissue by making supplementary cartilage loading information available to guide future research and development. Strain gauges have been successfully used as *in vivo* load sensors by attaching them directly to bone in animals and patients.[34–37] Recently, strain sensors have been attached to implantable scaffolds to collect joint load measurements. The preliminary results of those studies suggest that strain gauges attached to scaffolds could be used to monitor the *in vivo* changes of joint loads during gait in a canine model.[38]

The goal of this study was to measure joint loads during benchtop testing using gauges attached to implantable scaffolds and to determine whether they can be used to accurately and reproducibly infer joint loads and pressures. An additional aim was to evaluate the effect of implanted scaffolds on stifle joint mechanics by examining surface pressure patterns near scaffolds with pressure sensitive films. Although canine patellofemoral surface pressures have been measured,[39–44] very little information about tibia–femoral joint pressure is currently available.

METHODS

Overall Approach

The carcasses of five adult mongrels were obtained according to an IACUC approved protocol. Both hind limbs from each dog were explanted and the stifle joints were excised, leaving the capsules and soft tissues intact. Additionally, the hind limbs of nine hounds, that had been part of a recently completed *in vivo* study to evaluate bone ingrowth into implanted polybutylene terephthalate (PBT) scaffolds and PBT scaffold biocompatibility, were obtained and explanted in a similar manner. Strain measurements were not taken from the *in vivo* test animals. All isolated joints were loaded using the same procedure with an MTS servo-hydraulic test machine (Materials Testing System, Minneapolis, MN) while strain gauges attached to the PBT scaffolds and pressure sensitive film were used to assess joint loading.

PBT Scaffold

A three-dimensional (3D) porous PBT scaffold design was created on a CAD program (SolidWorks, Concord, MA) using a previously reported method.[45] Cylindrical scaffolds (9.5

mm diameter) had a domed top, where the radius of curvature (8 mm) of the flattened dome was chosen to approximate the curvature of the medial femoral condyle [Figure 1(A)]. Three sets of holes (0.5 mm diameter, 1 mm depth) spaced 120° apart were placed perpendicular to the scaffold's long axis to facilitate bone ingrowth through the sides of the scaffold [Figure 1 (A)]. Equidistant cutouts were placed around the base of the scaffold to accommodate strain gauge wiring [Figure 1(B)]. The interior of the scaffold was prepared so that it was porous through the base to encourage bone ingrowth and solid at the dome to support a tissue-engineered cartilage layer (Figure 1). A strand of polymer surrounded the exterior to transfer load to the strain gauges. Once completed, the 3D model was exported in a stereolithography format and uploaded into QuickSlice (Microsoft, Redmond, WA), the processing software for the Stratasys FDM 1650 fused deposition modeler (Stratasys, Eden Prairie, MN). Scaffolds were made with solid layers between the cylindrical portion and dome [Figure 1(C)]. This design was chosen to prevent vascular invasion of the dome, where the tissue-engineered cartilage layer would ultimately be grown in future experiments.

Gauge Attachment and Coating

Three 1000-Ω strain gauges (EA-06-125BT-120 Measurements Group, Raleigh, NC) were aligned along the long axis of the scaffold and attached with masterbond, an implantable grade of epoxy (EP42HT, Master Bond, Hackensack, NJ), around the circumference of each 9-mm cylindrical PBT porous scaffold (Figure 2). The gauge wires were positioned in slots located at the base of the scaffold, which prevented the wires from interfering with scaffold placement during implantation while providing sufficient porosity for bone ingrowth. The epoxy, used for gauge attachment, was cured for 24 h and each scaffold was tested for functionality and calibrated.

During the calibration process each scaffold was placed into a polyurethane foam holder. These foam constructs have previously been reported to have a compressive modulus similar to that of trabecular bone.[46] In each case, the foam holder and scaffold were compressed between the MTS loading plate and a layer of silicone at load rates of 50, 100, 150, and 200 N/s at peak loads up to 150 N. Scaffolds were loaded and then rotated 90° relative to the scaffold's long axis before being tested again to determine the effect of scaffold orientation in the foam. Strain measurements were recorded during both compression and relaxation. Loads from the MTS load cell and strains were measured simultaneously and load *versus* strain curves were plotted for each gauge. A calibration equation was determined for each scaffold, based on the load *versus* strain plots, in the form of the linear equation: $L = m \times S + b$, where L is the load in newtons, m the linear best fit slope, S the strain in microstrain, and b the calibration offset. To determine the influence that support structure stiffness had on the calibration relations, silicone structures of three different stiffnesses were tested.

Scaffold Placement

In both surgery and benchtop scaffold placement, a guide bit was drilled into the face of the medial condyle. The bit passed through the mid-diaphysis of the lateral aspect of the femur to allow the cable from the scaffold to exit at this location. A 9-mm reamer was used to ream into the face of the condyle to the depth of the height of the scaffold (2 cm). The reamer and guide bit were removed, leaving a space for the scaffold and a hole to guide the gauge wires through the condyle to the lateral aspect of the femur. The wires were passed through the guide bit hole and the scaffold was seated into the medial condyle, leaving the dome of the scaffold flush with the articulating surface[38] (Figure 3). To allow sufficient bone ingrowth, scaffolds from the *in vivo* study were left in place for ~6 months prior to the killing of the animals and removal of their limbs for testing.

Joint Preparation

Each limb was cut just distal to the femoral neck and proximal to the hock, leaving ~75% of the tibia. Holes were drilled transversely through both cut bone ends, which allowed a gauge wire (no. 14) to be threaded through the bone, preventing loosening of the bone once it was mounted on the MTS. The bone ends were fixed in 5-cm sections of copper tubing (2.5 cm diameter) using quicksetting epoxy (Devcon, Danvers, MA). The copper tubing was then attached securely to a loading fixture (Figure 4) connected to the MTS.

After attaching the stifle joints to the loading fixture, the posterior portion of both right and left joint capsules were incised and the collateral ligaments were severed. The cruciate ligaments and the patellar tendon were left intact and the proximal portion of the patellar tendon was attached to a 5-N weight. The bones of five mongrels received scaffolds on the benchtop. The nine sets of hound bones from the *in vivo* study had received scaffolds during sterile surgery using a similar procedure. Left knees of both groups did not receive scaffolds and were used as controls.

Joint Loading

Loads up to 130 N were applied to joints at load rates of 50, 100, 150, and 200 N/s. Loading was carried out with joints at 30°, 50°, and 70° flexion to simulate paw strike, stance, and toe off during gait[47] (Figure 5). At each flexion angle, pressure sensitive impressions were taken, scanned, and analyzed five times. Loads and strains were recorded at 100 samples/s and saved to a spreadsheet. Low-pressure high-sensitivity films (Super Low Film two sheet type, Pressurex Film, Hanover, NJ) were cut into 2.5 × 5 cm^2 strips. The films were connected with transparent tape to form a two-part film packet that did not allow fluid infiltration. Film packets were placed into both medial and lateral compartments of the joint before being loaded. Three sets of mongrel joints were tested with pressure sensitive film before and after placing the scaffold. In one other mongrel, one scaffold was placed slightly protruding from the femoral surface in order to determine the effect of inadequately seated scaffolds on peak surface pressure in the joint. In the remaining two sets of mongrel joints, scaffolds were placed, tested, and then rotated with respect to the long axis in order to change the orientation of the scaffolds in the drill hole of the femoral condyle.

Data Analysis

Pressure sensitive films were scanned using a LaCie Silver-scanner II at 400 dpi and imported into ImageJ 1.4.2v software (NIH, Bethesda, MD. Artifacts, which were visually identified as marks located outside of the area of the outer perimeter of the menisci, were removed from the scanned images. Marks that were straight lines found on pressure films were considered to be crinkle artifacts and were also removed. Images were converted and scaled to a range of 0–255 (0 = white, 255 = black). Peak pressures were determined by applying pixel density conversion algorithms derived from calibration graphs provided by Pressurex® pressure sensitive films. Strain measurements from strain-gauged scaffolds were converted to loads using scaffold calibration coefficients determined during the calibration loading procedure. For all the analyses a nonparametric Kendall's W test, equivalent to a dependent *t* test, was used to determine significance at a p value of 0.05.

RESULTS

Strain-Gauged Scaffold Calibration

Strain *versus* load curves for gauged scaffolds were consistently linear throughout the range of loads applied during the calibration process (Figure 6). Within physiological loading rates,[47] changes in calibrations were insignificant (Kendall's W: $p = 0.495$) (Table I). Changing

scaffold orientation provided an insignificant change in the linear coefficients of the load/strain calibration relations (Kendall's W: $p = 0.146$), and an insignificant change was noted when silicone layers of different elastic moduli were used in the calibration process (Kendall's W: $p = 0.779$) (Table I). However, a significant variation of coefficients was apparent when comparing calibration relation equations from one strain-gauged scaffold with those from the next.

Pressure Sensitive Film

Similar maximum contact surface pressures, measured using pressure sensitive film, were obtained before and after scaffold placement (Figure 7). On the joint surface of the nine hounds, peak pressures at 30° of flexion ranged from 0.91 to 2.36 MPa on the medial surface and 0.86 to 2.43 MPa on the lateral surface (Table II). At 50° of flexion, the medial surface pressures ranged from 0.97 to 2.43 MPa, whereas the lateral surface pressures ranged from 0.85 to 2.02 MPa (Table II). Peak pressures at 70° of flexion ranged from 1.01 to 2.53 MPa on the medial surface and 1.07 to 2.29 MPa on the lateral surface (Table II). Figure 8 shows the peak pressures from the medial surface of all joints at 30° of flexion. Thirty degrees of flexion is of particular interest because the condyle area containing the implanted scaffold is most directly loaded and at this angle load transmission is most closely aligned along the axis of loading of the strain gauges. Changes in peak pressures between control and test knees were nonsignificant ($p = 0.452$).

Markedly increased maximum surface pressures were detected using pressure sensitive films in the mongrel stifle joint where the scaffold was placed relatively proud to the condyle surface (Figure 9).

Strain-Gauged Scaffold Measurements

Strain measurements were consistently and repeatedly acquired from all strain-gauged scaffolds during compression loading of the stifles. Loads as small as 2.5 N, applied to the joints, produced detectable changes in measured strains corresponding to the change in applied loads. Both cyclic and sustained loads were reliably monitored through the strain-gauged scaffold systems. Scaffold orientation did affect gauge reading consistency in implanted scaffolds. In one scaffold at the initial placement orientation, all three gauges inferred similar loads (39.72 ± 1.17 N) based on strain measurements, yielding a coefficient of variance of 2.95%. When the scaffold was tested and then rotated 90°, inferred loads yielded a coefficient of variance of 12.67% (15.03 ± 1.90 N).

DISCUSSION

This study demonstrated that strain measurements from gauged scaffolds reliably correspond to applied loads acting on the femoral condyles in both magnitude and duration. It also established normal surface pressures on the canine tibia–femoral joint and the nominal effect of scaffold placement on stifle joint pressures. Throughout the duration of the study, individual scaffold calibrations proved to be consistent. This consistent linear calibration relationship between load and strain insured a simple interpretation of measurements collected within the physiological load range. The variance of calibration coefficients from one strain-gauged scaffold to the next can be attributed to the distinct characteristics of each gauge and the slight variations in material properties of the PBT composite in each scaffold. This difference of coefficients can be accounted for by individual scaffold calibrations and applying those calibrations to strain measurements of that particular scaffold to infer load transmission through the scaffold.

Innate to any cartilage repair procedure is the risk of altering joint mechanics, leading to damage of the surrounding native tissue. A meniscectomy, for example, reduces joint contact area surface, causing dramatic increases in peak contact stress.[48–51] The increased surface pressure has frequently led to the premature development of osteoarthritis.[52–54] Recently, implants used in meniscal repair procedures have led to significant increases in peak joint pressures, initiating femoral cartilage damage.[43] Pressure sensitive films have been widely used in joint mechanic experiments to analyze surface stress[55–61] and were used in this study to validate the normal pressures of the knee joint as well as determining the effects of scaffold implantation. Contact joint pressures measured in this study were comparable to those previously reported.[62,63] A comparison of joint pressures, with and without scaffold placement, indicated that the scaffold placement procedure did not significantly alter contact pressures. The lower pressures measured in both medial and lateral condyles of the experimental joint of specimen C7 (0.67 MPa and 0.52 MPa), when compared with those of the control, may be attributed to disparities of the stifle joints of the test animal.[64] It is also possible that the scaffold was improperly placed, slightly altering the mechanics of the knee and reducing the peak load on the medial surface. Although care was taken to select animals of similar size and breed, the variability of pressures noted when comparing the results of one test animal with those of another may be attributed to the minor anatomical differences of the test animals.

Additional concerns about the impact of the implanted scaffold would need to be addressed before proceeding to clinical trials. One major concern would be the effect of the engineered tissue articulating against the healthy tibial plateau and meniscus. Although the scaffolds placed in the *in vivo* trials did not have the tissue engineered cartilage layer to be placed in future trials, when the scaffolds were accurately placed no gross evidence of cartilage surface damage on either the tibial or meniscal surface could be seen when examined with a stereomicroscope. Currently, examination of the cartilage surface to detect subsurface damage using optical coherence tomography, SEM, and hard tissue histology staining techniques are being developed. These techniques will also be used to compare the native tissues with the engineered tissue layer. Another major concern of implant procedures is the occurrence of infection due to the implantation of the scaffolds, strain gauges, or wires. As reported,[38] none of the *in vivo* test animals that received scaffolds showed signs of synovitis or infection at any of the sites involved in the surgical placement of wires or scaffolds. This is consistent with previously published work looking at the effect of implanted strain gauges,[35–37] cables,[35] and radio transmitters.[32]

Throughout the study strain measurement fidelity was found to be greatest at 30° of flexion, which corresponds to push off during gait. This was likely due to the design and orientation of the strain gauges on the scaffolds. Strain gauges used in this study were limited to sensing along a single axis, and the implanted gauges were most closely aligned with the 30° flexion angle. Although beyond the scope of this study, future benchtop development may benefit from the use of multiple gauges oriented along various axes to allow strain sensing in three dimensions. This would allow measurements over a broader range of angles and may facilitate tangential shear detection.

The reproducibility of the strain measurements and ease of load analysis from the strain-gauged scaffolds make this system ideal for consideration in an *in vivo* model. The 2.5-N sensitivity calculated in this study is more than adequate for joint load measurement. During *in vivo* experiments, bone growth into scaffold pores will fix scaffolds securely in place. Once fixed in place, loads on condyles may more fastidiously compress the scaffold, resulting in a higher strain measurement accuracy. Evaluation of these *in vivo* effects was beyond the scope of this study. However, this situation could potentially be modeled by cementing scaffolds in place in a benchtop experiment or conversely by monitoring scaffolds *in vivo* over extended periods

while bone ingrowth occurs. The PBT material used to create the scaffolds used in this study is marginally degradable. Preliminary results of a degradation study[65] indicate that PBT scaffolds do not begin to lose their mechanical properties for at least 1 year *in vivo*. This will provide the engineered cartilage substantial time to heal and integrate with the surrounding tissue.

Results from this study imply that a strain-gauged scaffold measurement system has the attributes necessary for animal studies and eventually clinical trials because of the uniformity of calibration relationships at load rates within the physiological range. This further indicates that strain-gauged scaffolds can be used to collect measurements in test animals and in patients when they are standing, walking, and running. The consistency of measurements to cyclic and sustained loads suggests that this measurement system is robust and can generally be applied to studies in animals or patients. Material properties of joints can vary within a patient population or within an individual joint depending on location.[66–69] Scaffold calibration relations remained consistent over a range of silicone stiffness, suggesting that calibration algorithms will accurately measure loads in a wide range of locations in test animals and patients.

Measurements collected *in vivo* may have both clinical and experimental relevance. Currently no measurements exist that show cartilage loading during various impact generating activities such as kneeling, stair climbing, and jumping. These measurements will help determine native cartilage tissue environments and can provide standards for both peak loads and loading rates in the testing of engineered cartilage products. Once the native cartilage loads have been established, monitoring of joint loads can aid rehabilitation by warning patients of joint overloading. Additionally, clinical practitioners could use real time measurements to guide rehabilitation. An understanding of healthy cartilage loading can provide key insights to investigators trying to establish the relationship between mechanical loads and chondrocyte functionality. A better understanding of loading regimens during various activities may help cartilage biologists determine activation loads that lead to a positive chondrocyte response.

CONCLUSIONS

The novel scaffold system tested in this study gives rise to a new dimension of scaffold-based cartilage engineering by adding a diagnostic element. Scaffold calibrations relating strain and applied loads were consistent and repeatable, allowing the scaffolds to reliably detect load transmission in the knee. Pressure sensitive film analysis was used to determine joint pressures and indicated that the scaffold itself did not influence the peak contact pressures on the joint.

Real-time monitoring of joint loading has the potential to provide important clinical and diagnostic information such as a complete joint loading history during the postsurgery period. It also has the potential to add fundamental insights into the native environment of the knee joint. Clinical studies may possibly use strain-gauged scaffolds to establish normal joint loads and to determine loads that are damaging to both healthy and tissue-engineered cartilage. This could aid physicians in determining appropriate knee therapies and will be paramount in the development of a functional engineered cartilage tissue.

Acknowledgements

The authors thank Corina Fuentes, funded through Western Alliance to Expand Student Opportunities (WAESO), and Chris Geffre, funded through the University of Arizona's Undergraduate Biology Research Program (UBRP), for their help with this study, and Kristy Bliss for her copyediting.

Contract grant sponsor: The National Institute of Health (NIH)

Contract grant Sponsor: National Institute of Biomedical Imaging and BioEngineering (NIBIB); contract grant number: RO1-EB000660

References

1. Guilak F, Butler DL, Goldstein SA. Functional tissue engineering: The role of biomechanics in articular cartilage repair. Clin Orthop Relat Res 2001;391(Suppl):S295–S305. [PubMed: 11603713]
2. Hangody L. The mosaicplasty technique for osteochondral lesions of the talus. Foot Ankle Clin 2003;8:259–273. [PubMed: 12911240]
3. Bentley G, Biant LC, Carrington RW, Akmal M, Goldberg A, Williams AM, Skinner JA, Pringle J. A prospective, randomised comparison of autologous chondrocyte implantation versus mosaicplasty for osteochondral defects in the knee. J Bone Joint Surg Br 2003;85:223–230. [PubMed: 12678357]
4. Huntley JS, Bush PG, McBirnie JM, Simpson AH, Hall AC. Chondrocyte death associated with human femoral osteochondral harvest as performed for mosaicplasty. J Bone Joint Surg Am 2005;87:351–360. [PubMed: 15687159]
5. Gross AE. Cartilage resurfacing: Filling defects. J Arthroplasty 2003;18(3 Suppl 1):14–17. [PubMed: 12730921]
6. Hangody L, Rathonyi GK, Duska Z, Vasarhelyi G, Fules P, Modis L. Autologous osteochondral mosaicplasty. Surgical technique J Bone Joint Surg Am 2004;A86(Suppl 1):65–72.
7. Brittberg M, Lindahl A, Nilsson A, Ohlsson C, Isaksson O, Peterson L. Treatment of deep cartilage defects in the knee with autologous chondrocyte transplantation. N Engl J Med 1994;331:889–895. [PubMed: 8078550]
8. Ocelus SM. Autologous cultured chondrocytes for the treatment of knee cartilage injury. Orthop Nurs 2000;19:19–27. [PubMed: 11153318]quiz 27–29
9. Peterson L, Minas T, Brittberg M, Nilsson A, Sjogren-Jansson E, Lindahl A. Two- to nine-year outcome after autologous chondrocyte transplantation of the knee. Clin Orthop Relat Res 2000;374:212–234. [PubMed: 10818982]
10. Horas U, Pelinkovic D, Herr G, Aigner T, Schnettler R. Autologous chondrocyte implantation and osteochondral cylinder transplantation in cartilage repair of the knee joint. A prospective, comparative trial J Bone Joint Surg Am 2003;A85(Suppl 2):185–192.
11. Jerosch J, Filler T, Peuker E. Is there an option for harvesting autologous osteochondral grafts without damaging weight-bearing areas in the knee joint? Knee Surg Sports Traumatol Arthrosc 2000;8:237–240. [PubMed: 10975265]
12. Woodfield TB, Bezemer JM, Pieper JS, van Blitterswijk CA, Riesle J. Scaffolds for tissue engineering of cartilage. Crit Rev Eukaryot Gene Expr 2002;12:209–236. [PubMed: 12449344]
13. Uematsu K, Hattori K, Ishimoto Y, Yamauchi J, Habata T, Takakura Y, Ohgushi H, Fukuchi T, Sato M. Cartilage regeneration using mesenchymal stem cells and a three-dimensional poly-lactic-glycolic acid (PLGA) scaffold. Biomaterials 2005;26:4273–4279. [PubMed: 15683651]
14. Meinel L, Hofmann S, Karageorgiou V, Zichner L, Langer R, Kaplan D, Vunjak-Novakovic G. Engineering cartilage-like tissue using human mesenchymal stem cells and silk protein scaffolds. Biotechnol Bioeng 2004;88:379–391. [PubMed: 15486944]
15. Solchaga LA, Temenoff JS, Gao J, Mikos AG, Caplan AI, Goldberg VM. Repair of osteochondral defects with hyaluronan-and polyester-based scaffolds. Osteoarthritis Cartilage 2005;13:297–309. [PubMed: 15780643]
16. Pavesio A, Abatangelo G, Borrione A, Brocchetta D, Hollander AP, Kon E, Torasso F, Zanasi S, Marcacci M. Hyaluronan-based scaffolds (Hyalograft C) in the treatment of knee cartilage defects: Preliminary clinical findings. Novartis Found Symp 2003;249:203–217. [PubMed: 12708658] discussion 229–233, 234–238, 239–241
17. Capito RM, Spector M. Scaffold-based articular cartilage repair. IEEE Eng Med Biol Mag 2003;22:42–50. [PubMed: 14699935]
18. Griffon DJ, Sedighi MR, Sendemir-Urkmez A, Stewart AA, Jamison R. Evaluation of vacuum and dynamic cell seeding of polyglycolic acid and chitosan scaffolds for cartilage engineering. Am J Vet Res 2005;66:599–605. [PubMed: 15900939]

19. Tamai N, Myoui A, Hirao M, Kaito T, Ochi T, Tanaka J, Takaoka K, Yoshikawa H. A new biotechnology for articular cartilage repair: Subchondral implantation of a composite of interconnected porous hydroxyapatite, synthetic polymer (PLA-PEG), and bone morphogenetic protein-2 (rhBMP-2). Osteoarthritis Cartilage 2005;13:405–417. [PubMed: 15882564]
20. Veilleux N, Spector M. Effects of FGF-2 and IGF-1 on adult canine articular chondrocytes in type II collagen-glycosaminoglycan scaffolds in vitro. Osteoarthritis Cartilage 2005;13:278–286. [PubMed: 15780641]
21. Ma Z, Gao C, Gong Y, Shen J. Cartilage tissue engineering PLLA scaffold with surface immobilized collagen and basic fibroblast growth factor. Biomaterials 2005;26:1253–1259. [PubMed: 15475055]
22. Saha AK, Mazumdar J, Kohles SS. Prediction of growth factor effects on engineered cartilage composition using deterministic and stochastic modeling. Ann Biomed Eng 2004;32:871–879. [PubMed: 15255217]
23. Huang Q, Goh JC, Hutmacher DW, Lee EH. In vivo mesenchymal cell recruitment by a scaffold loaded with transforming growth factor β1 and the potential for in situ chondrogenesis. Tissue Eng 2002;8:469–482. [PubMed: 12167232]
24. Fujisato T, Sajiki T, Liu Q, Ikada Y. Effect of basic fibroblast growth factor on cartilage regeneration in chondrocyte-seeded collagen sponge scaffold. Biomaterials 1996;17:155–162. [PubMed: 8624392]
25. Naughton GK. From lab bench to market: Critical issues in tissue engineering. Ann NY Acad Sci 2002;961:372–385. [PubMed: 12081943]
26. Strehl R, Tallheden T, Sjogren-Jansson E, Minuth WW, Lindahl A. Long-term maintenance of human articular cartilage in culture for biomaterial testing. Biomaterials 2005;26:4540–4549. [PubMed: 15722123]
27. Sharma B, Elisseeff JH. Engineering structurally organized cartilage and bone tissues. Ann Biomed Eng 2004;32:148–159. [PubMed: 14964730]
28. Radder AM, Leenders H, van Blitterswijk CA. Interface reactions to PEO/PBT copolymers (Polyactive) after implantation in cortical bone. J Biomed Mater Res 1994;28:141–151. [PubMed: 8207024]
29. Roessler M, Wilke A, Griss P, Kienapfel H. Missing osteoconductive effect of a resorbable PEO/PBT copolymer in human bone defects: A clinically relevant pilot study with contrary results to previous animal studies. J Biomed Mater Res 2000;53:167–173. [PubMed: 10713563]
30. Szivek JA, Margolis DS, Garrison BK, Nelson E, Vaidyanathan RK, DeYoung DW. TGF-β1-enhanced TCP-coated sensate scaffolds can detect bone bonding. J Biomed Mater Res B: Appl Biomater 2005;73:43–53. [PubMed: 15682399]
31. Yang X, Tare RS, Partridge KA, Roach HI, Clarke NM, Howdle SM, Shakesheff KM, Oreffo RO. Induction of human osteoprogenitor chemotaxis, proliferation, differentiation, and bone formation by osteoblast stimulating factor-1/pleiotrophin: Osteoconductive biomimetic scaffolds for tissue engineering. J Bone Miner Res 2003;18:47–57. [PubMed: 12510805]
32. Szivek JA, Roberto RF, Slack JM, Majeed BS. An implantable strain measurement system designed to detect spine fusion: Preliminary results from a biomechanical in vivo study. Spine 2002;27:487–497. [PubMed: 11880834]
33. Butler DL, Shearn JT, Juncosa N, Dressler MR, Hunter SA. Functional tissue engineering parameters toward designing repair and replacement strategies. Clin Orthop Relat Res 2004;427(Suppl):S190–S199. [PubMed: 15480066]
34. Lanyon LE, Hampson WG, Goodship AE, Shah JS. Bone deformation recorded in vivo from strain gauges attached to the human tibial shaft. Acta Orthop Scand 1975;46:256–268. [PubMed: 1146518]
35. Szivek JA, Anderson PL, DeYoung DW. In vivo strain measurements collected using calcium phosphate ceramic-bonded strain gauges. J Invest Surg 1997;10:263–273. [PubMed: 9361990]
36. Cordaro NM, Weiss JA, Szivek JA. Strain transfer between a CPC coated strain gauge and cortical bone during bending. J Biomed Mater Res 2001;58:147–155. [PubMed: 11241333]
37. Rabkin BA, Szivek JA, Schonfeld JE, Halloran BP. Long-term measurement of bone strain in vivo: The rat tibia. J Biomed Mater Res 2001;58:277–281. [PubMed: 11319741]

38. Szivek, JA.; Bliss, CL.; Ruth, JT.; Schnepp, AB.; DeYoung, DW.; Vaidyanathan, RK. An instrumented scaffold to monitor loading of cartilage in the knee joint. 51st Annual Meeting of the ORS Transactions; Washington, DC. Feb 20–23, 2005; Poster No. 471
39. Elias JJ, Wilson DR, Adamson R, Cosgarea AJ. Evaluation of a computational model used to predict the patellofemoral contact pressure distribution. J Biomech 2004;37:295–302. [PubMed: 14757448]
40. Atkinson PJ, Ewers BJ, Haut RC. Blunt injuries to the patellofemoral joint resulting from transarticular loading are influenced by impactor energy and mass. J Biomech Eng 2001;123:293–295. [PubMed: 11476374]
41. Thompson RC Jr, Oegema TR Jr, Lewis JL, Wallace L. Osteoarthrotic changes after acute transarticular load: An animal model. J Bone Joint Surg Am 1991;73:990–1001. [PubMed: 1714911]
42. LaBerge M, Audet J, Drouin G, Rivard CH. Structural and in vivo mechanical characterization of canine patellar cartilage: A closed chondromalacia patellae model. J Invest Surg 1993;6:105–116. [PubMed: 8512885]
43. Chan KM, Qin L, Hung LK, Tang CY, Li CK, Rolf C. Alteration of patellofemoral contact during healing of canine patellar tendon after removal of its central third. J Biomech 2000;33:1441–1451. [PubMed: 10940403]
44. Clark AL, Herzog W, Leonard TR. Contact area and pressure distribution in the feline patellofemoral joint under physiologically meaningful loading conditions. J Biomech 2002;35:53–60. [PubMed: 11747883]
45. Vaidyanathan, RK.; Green, C.; Bourque, P.; Calvert, PD.; Szivek, JA.; Maxian, SH. Strong porous polymer-ceramic composites by rapid prototyping for resorbable orthopedic scaffold applications. Society for Biomaterials; Tampa FL: Mar. 2002
46. Szivek JA, Thompson JD, Benjamin JB. Characterization of three formulations of a synthetic foam as models for a range of human cancellous bone types. Journal of Applied Biomaterials 1995;6:125–128. [PubMed: 7640439]
47. Nunamaker, DM.; Blauner, PD. Textbook of Small Animal Orthopaedics. Ithaca, NY: J. B. Lippincott; 1985.
48. Schreppers GJ, Sauren AA, Huson A. A numerical model of the load transmission in the tibio-femoral contact area. Proc Inst Mech Eng [H] 1990;204:53–59.
49. Donahue TL, Hull ML, Rashid MM, Jacobs CR. A finite element model of the human knee joint for the study of tibiofemoral contact. J Biomech Eng 2002;124:273–280. [PubMed: 12071261]
50. Lee TQ, Morris G, Csintalan RP. The influence of tibial and femoral rotation on patellofemoral contact area and pressure. J Orthop Sports Phys Ther 2003;33:686–693. [PubMed: 14669964]
51. Allen PR, Denham RA, Swan AV. Late degenerative changes after meniscectomy. Factors affecting the knee after operation. J Bone Joint Surg Br 1984;66:666–671. [PubMed: 6548755]
52. Krause WR, Pope MH, Johnson RJ, Wilder DG. Mechanical changes in the knee after meniscectomy. J Bone Joint Surg Am 1976;58:599–604. [PubMed: 946970]
53. Newman AP, Anderson DR, Daniels AU, Jee KW. The effect of medial meniscectomy and coronal plane angulation on in vitro load transmission in the canine stifle joint. J Orthop Res 1989;7:281–291. [PubMed: 2918427]
54. McBride ID, Reid JG. Biomechanical considerations of the menisci of the knee. Can J Sport Sci 1988;13:175–187. [PubMed: 3064900]
55. Hale JE, Brown TD. Contact stress gradient detection limits of Pressensor film. J Biomech Eng 1992;114:352–357. [PubMed: 1522730]
56. Marder RA, Swanson TV, Sharkey NA, Duwelius PJ. Effects of partial patellectomy and reattachment of the patellar tendon on patellofemoral contact areas and pressures. J Bone Joint Surg Am 1993;75:35–45. [PubMed: 8419389]
57. Fukubayashi T, Kurosawa H. The contact area and pressure distribution pattern of the knee. A study of normal and osteo-arthrotic knee joints. Acta Orthop Scand 1980;51:871–879. [PubMed: 6894212]
58. Harris ML, Morberg P, Bruce WJ, Walsh WR. An improved method for measuring tibiofemoral contact areas in total knee arthroplasty: A comparison of K-scan sensor and Fuji film. J Biomech 1999;32:951–958. [PubMed: 10460132]
59. Agneskirchner JD, Hurschler C, Stukenborg-Colsman C, Imhoff AB, Lobenhoffer P. Effect of high tibial flexion osteotomy on cartilage pressure and joint kinematics: A biomechanical study in human

cadaveric knees. Winner of the AGA-DonJoy Award 2004. Arch Orthop Trauma Surg 2004;124:575–584. [PubMed: 15480717]

60. Takahashi T, Wada Y, Yamamoto H. Soft-tissue balancing with pressure distribution during total knee arthroplasty. J Bone Joint Surg Br 1997;79:235–239. [PubMed: 9119849]
61. Hasler EM, Herzog W, Fick GH. Appropriateness of plane pressure-sensitive film calibration for contact stress measurements in articular joints. Clin Biomech (Bristol, Avon) 1996;11:358–360.
62. Nelson BH, Anderson DD, Brand RA, Brown TD. Effect of osteochondral defects on articular cartilage. Contact pressures studied in dog knees. Acta Orthop Scand 1988;59:574–579. [PubMed: 3188865]
63. Brown TD, Pope DF, Hale JE, Buckwalter JA, Brand RA. Effects of osteochondral defect size on cartilage contact stress. J Orthop Res 1991;9:559–567. [PubMed: 2045983]
64. Brower A, Salamat S, Crawford J, Manley P. Unilateral limb enlargement in a dog with a malignant peripheral nerve sheath tumor. Vet Pathol 2005;42:353–356. [PubMed: 15872382]
65. Tellis BC, Szivek JA, Bliss CL, Margolis DS, Vaidyanathan RK, Calvert P. Trabecular scaffolds created using micro ct guided fused deposition modeling. Submitted to Journal Materials Science and Engineering Part C. April;2006
66. Lechner K, Hull ML, Howell SM. Is the circumferential tensile modulus within a human medial meniscus affected by the test sample location and cross-sectional area? J Orthop Res 2000;18:945–951. [PubMed: 11192255]
67. Csintalan RP, Schulz MM, Woo J, McMahon PJ, Lee TQ. Gender differences in patellofemoral joint biomechanics. Clin Orthop Relat Res 2002:260–269. [PubMed: 12218492]
68. Tonuk E, Silver-Thorn MB. Nonlinear viscoelastic material property estimation of lower extremity residual limb tissues. J Biomech Eng 2004;126:289–300. [PubMed: 15179861]
69. Jurvelin J, Kiviranta I, Tammi M, Helminen HJ. Effect of physical exercise on indentation stiffness of articular cartilage in the canine knee. Int J Sports Med 1986;7:106–110. [PubMed: 3754850]

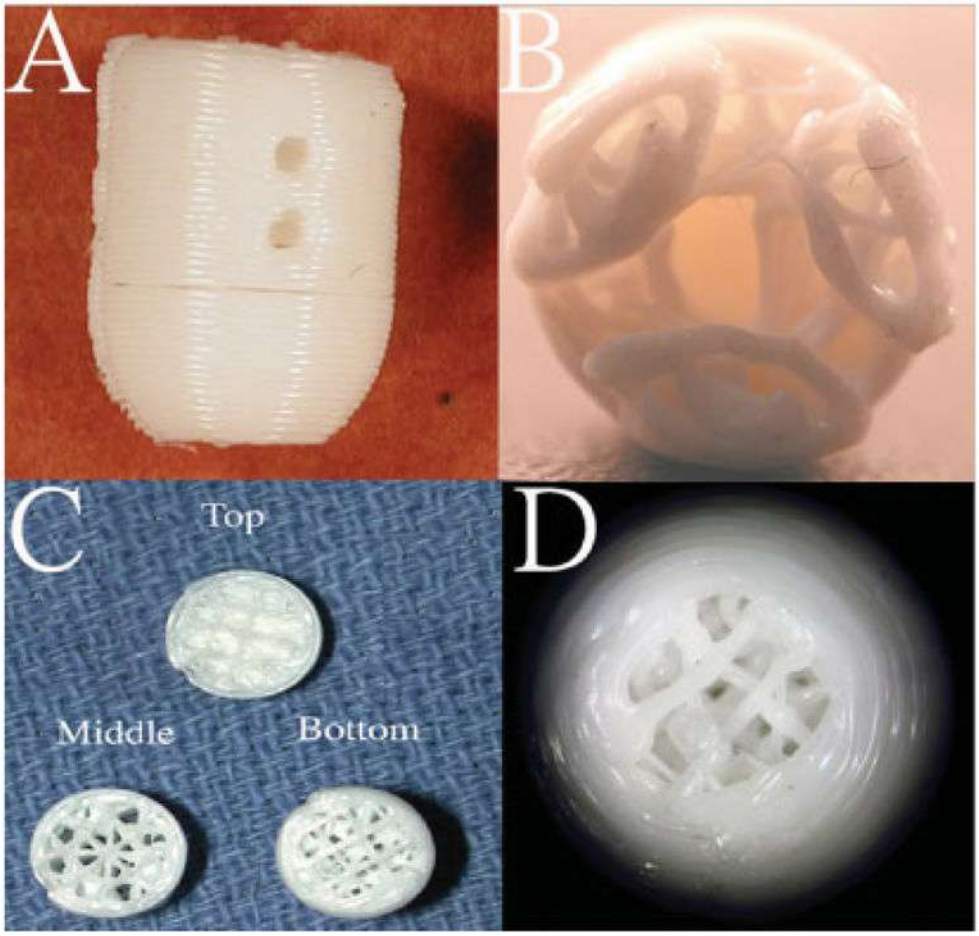

Figure 1.

A: Side view of a cylindrical PBT scaffold showing two holes designed for bone ingrowth. B: Bottom view of scaffold showing scaffold porosity and three cutouts for strain gauges. C: Sectional slices showing scaffold porosity throughout the scaffold layers and the solid layer in the top section to prevent vascular invasion of the tissue-engineered cartilage layer. D: Top view of scaffold showing the porous section where the tissue-engineered cartilage layer would be placed. [Color figure can be viewed in the online issue, which is available at www.interscience.wiley.com.]

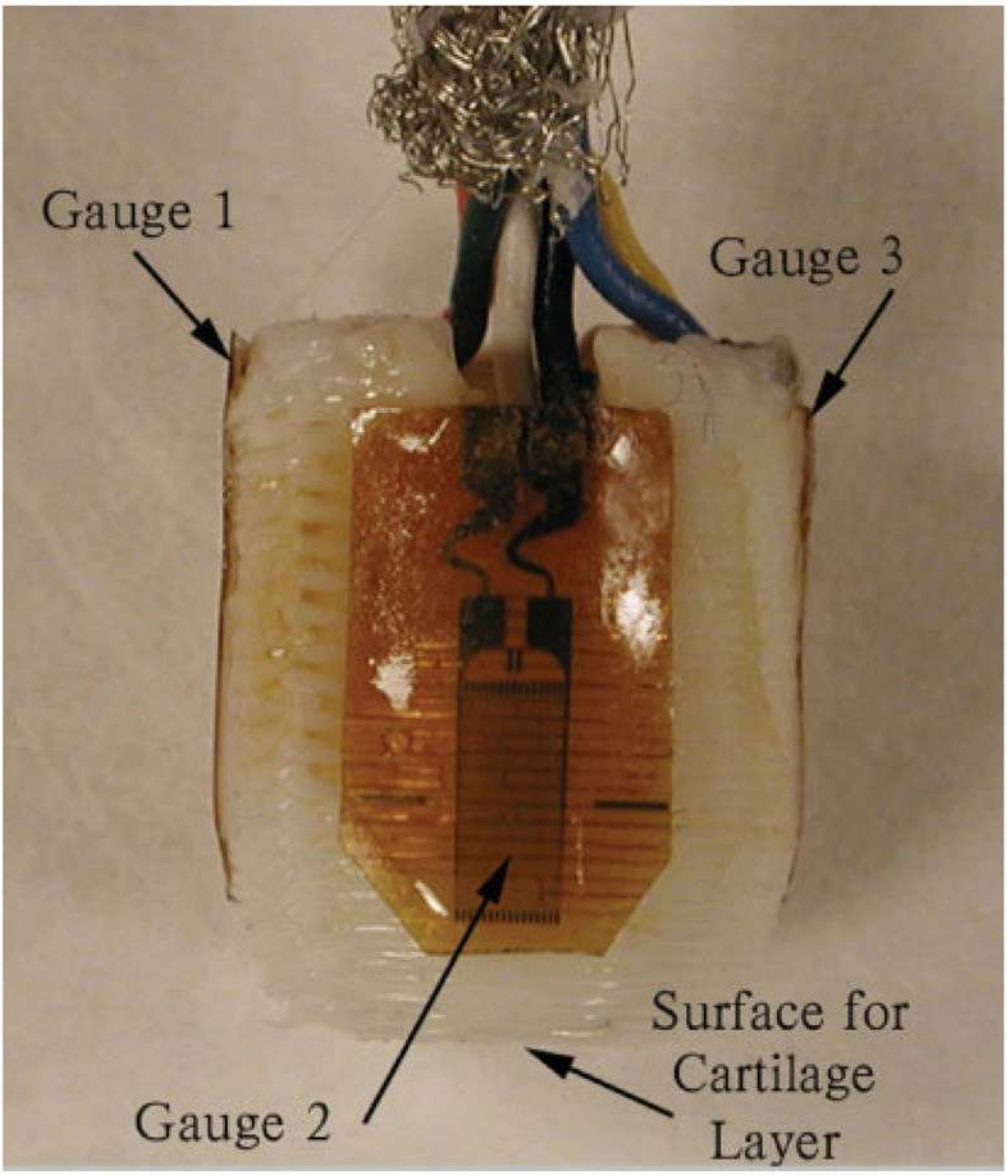

Figure 2.
Side view of a strain-gauged scaffold showing the face of one of three strain gauges. The thin polyamide backing of the remaining two gauges can be seen on either side of the scaffold. Arrows indicate the direction of expected bone ingrowth on the top and sides of the cylindrical scaffold. The tissue-engineered cartilage layer would be grown onto the dome at the bottom of the scaffold. [Color figure can be viewed in the online issue, which is available at www.interscience.wiley.com.]

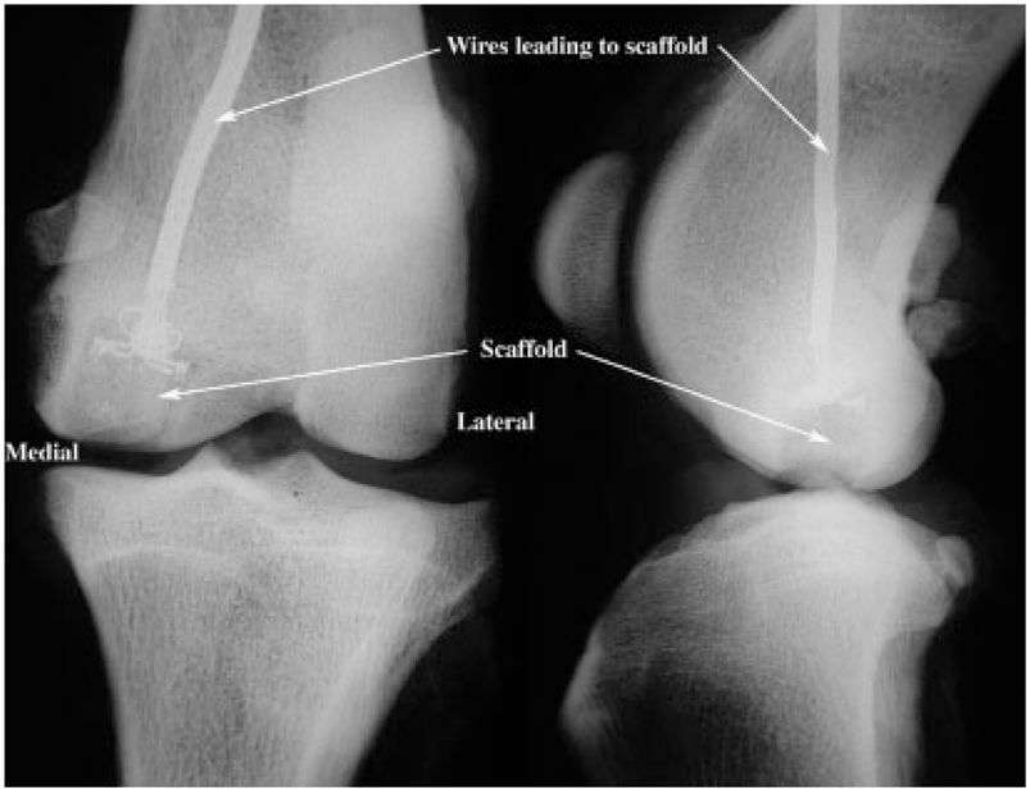

Figure 3.
Representative anterior/posterior (Left) and lateral (Right) radiographs of an implanted scaffold. Scaffold is placed in the medial femoral condyle flush with the articulating surface. Wires from the strain gauges attached to the scaffold pass through the bone and exit at the lateral aspect of the femur.

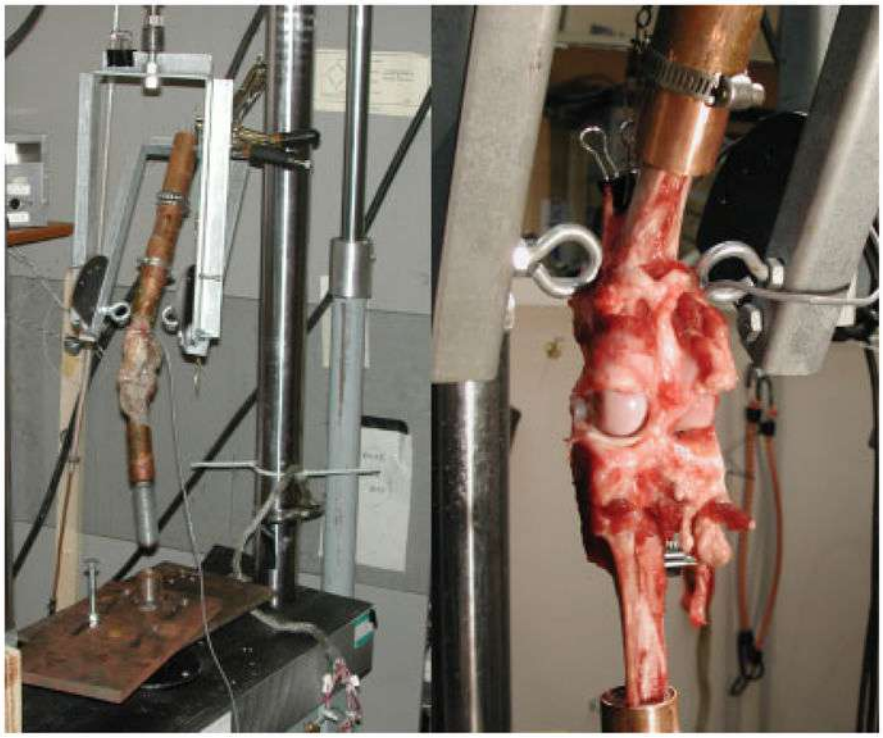

Figure 4.
Left: Intact canine stifle mounted into copper tubing and fixed into the MTS harness fixture. This fixture allows 30°, 50°, and 70° flexion of the joint during loading. Right: Posterior view of canine stifle with joint space exposed for pressure film placement. [Color figure can be viewed in the online issue, which is available at www.interscience.wiley.com.]

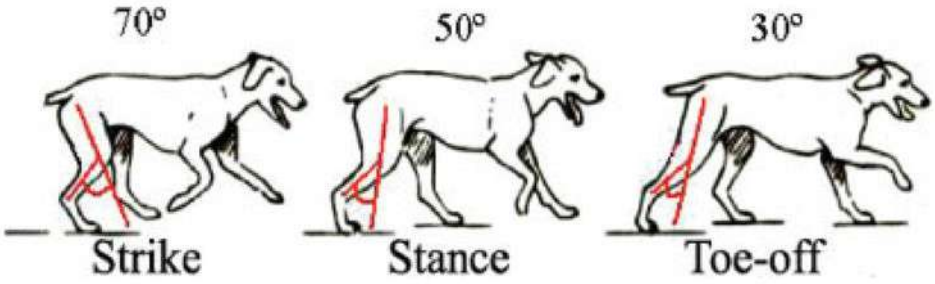

Figure 5.
Flexion angles were measured between the femur and the tibia. During the paw strike, the femur and tibia roughly form a 70° angle, whereas stance occurs at 50° flexion and toe-off (push-off) at 30°. [Color figure can be viewed in the online issue, which is available at www.interscience.wiley.com.]

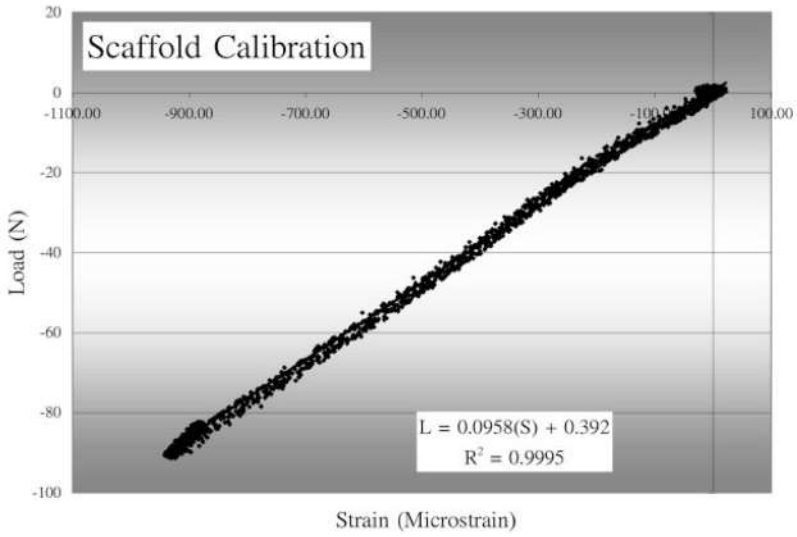

Figure 6.
A typical scaffold calibration curve showing linear relationship between load and strain. In the accompanying calibration equation, L indicates the load and S, the strain.

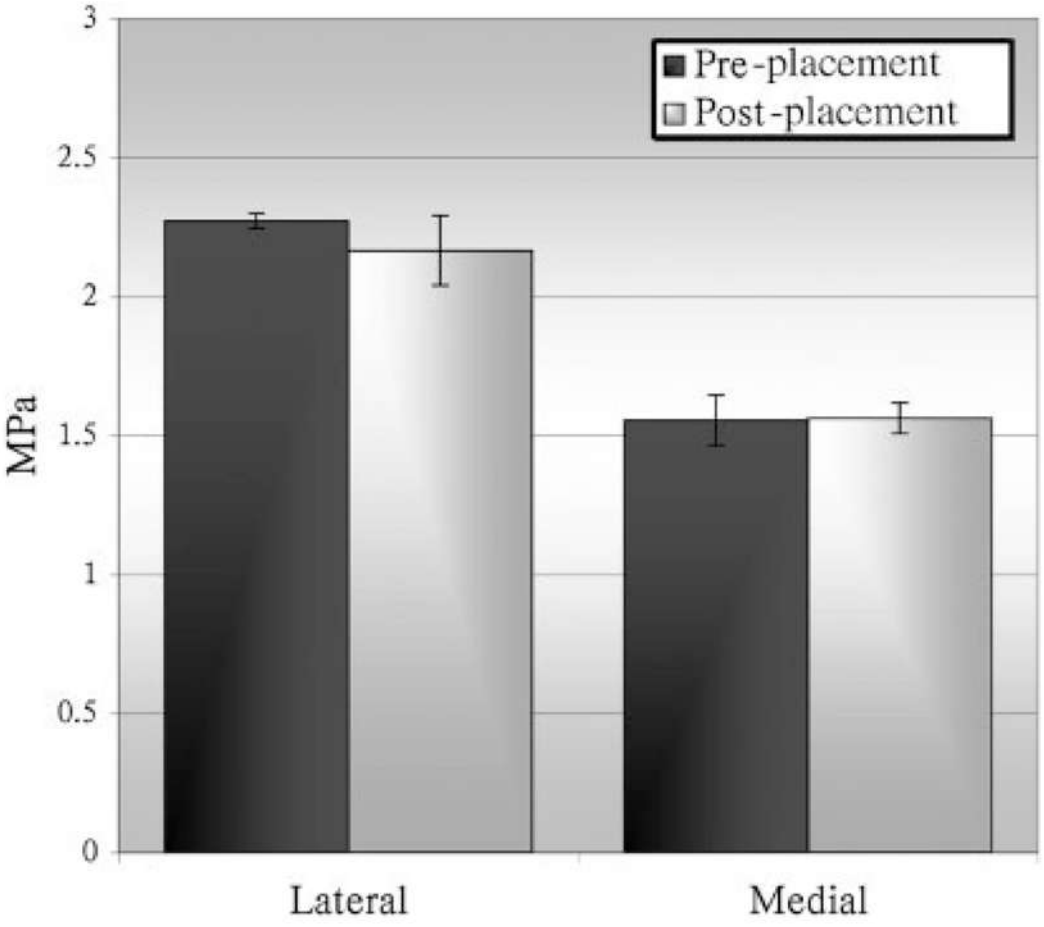

Figure 7.
Comparison of peak surface pressures measured before and after placement of a strain-gauged scaffold in one mongrel's joint.

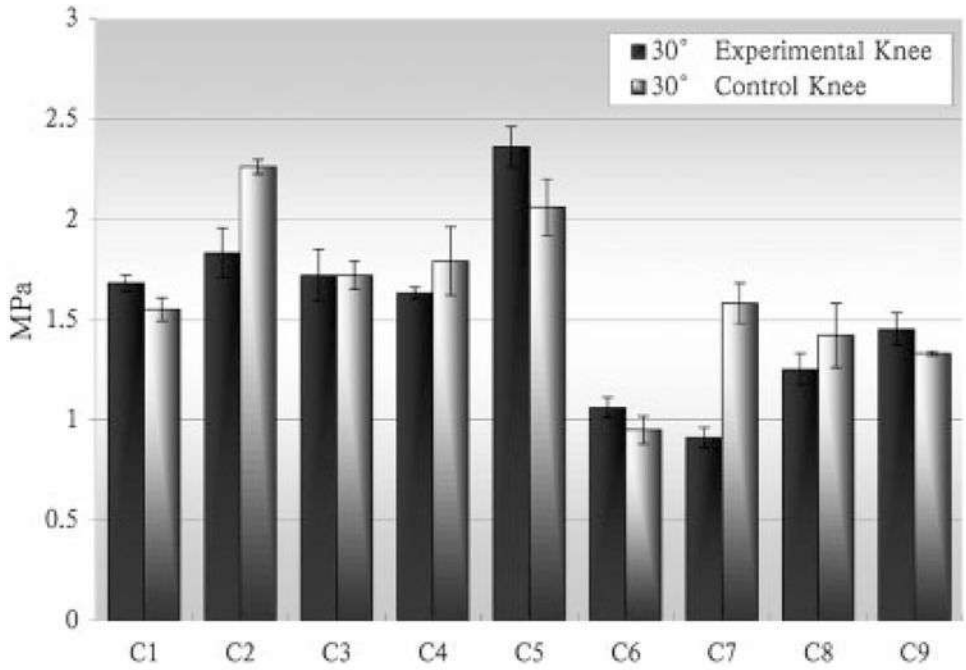

Figure 8.
Contact surface pressure measured from the medial joint surface in both right and left knees at 30° flexion.

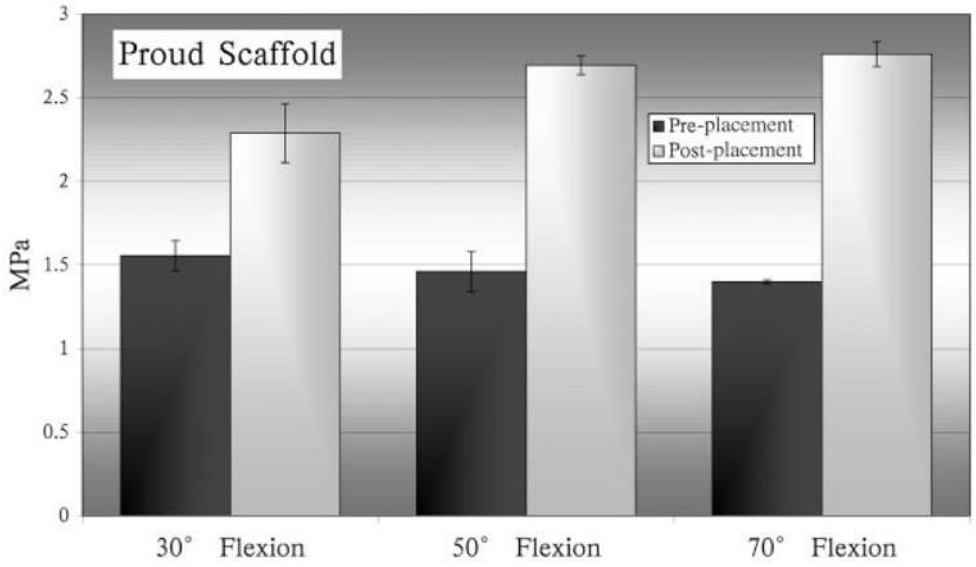

Figure 9.
Comparison of peak surface pressures measured before and after scaffold placement in one mongrel's joint. In this experiment, the scaffold was placed protruding from the surrounding cartilage layer.

TABLE I

Calibration Equation Comparison of Load Rates,[a] Orientation,[b] and Silicone Moduli[c]

	Gauge 1	Gauge 2	Gauge 3
Load rate (N/S)			
100	$L = 0.0172$ S	$L = 0.0202$ S	$L = 0.0196$ S
10	$L = 0.0169$ S	$L = 0.0188$ S	$L = 0.0195$ S
5	$L = 0.0177$ S	$L = 0.0189$ S	$L = 0.0195$ S
Orientation			
0°	$L = 0.0091$ S	$L = 0.0052$ S	$L = 0.0049$ S
90°	$L = 0.0091$ S	$L = 0.0055$ S	$L = 0.0045$ S
Silicone			
A	$L = 0.0181$ S	$L = 0.0141$ S	$L = 0.0212$ S
B	$L = 0.0242$ S	$L = 0.0156$ S	$L = 0.0222$ S
C	$L = 0.0169$ S	$L = 0.0188$ S	$L = 0.0195$ S

[a] Each scaffold has an individual calibration equation. The calibration coefficients for one scaffold at various loads rates. Silicone layer used: Silicone C.

[b] The values are those noted when a scaffold was calibrated, then rotated 90° and calibrated again.

[c] The calibration equations for one scaffold as the silicone layer used in the calibration process was varied.

TABLE II

Comparison of Peak Surface Pressures Measured in the Knee Joint in Which the Scaffold Was Placed (Experimental) and the Contralateral Joint Which Received No Scaffold (Control) of Each Test Animal at Three Different Flexion Angles

	Medial Pressure (MP ± SD)		Lateral Pressure (MP ± SD)	
Canine	**Experiment**	**Control**	**Experiment**	**Control**
At 30° flexion				
C1	1.68 ± 0.04	1.55 ± 0.06	1.64 ± 0.14	0.92 ± 0.06
C2	1.83 ± 0.12	2.26 ± 0.04	1.98 ± 0.05	1.22 ± 0.05
C3	1.72 ± 0.13	1.72 ± 0.07	1.75 ± 0.19	1.39 ± 0.13
C4	1.63 ± 0.03	1.79 ± 0.17	1.60 ± 0.01	0.86 ± 0.07
C5	2.36 ± 0.10	2.06 ± 0.14	1.34 ± 0.09	2.34 ± 0.05
C6	1.06 ± 0.05	0.95 ± 0.07	1.63 ± 0.07	2.32 ± 0.04
C7	0.91 ± 0.05	1.58 ± 0.10	1.36 ± 0.13	1.88 ± 0.09
C8	1.25 ± 0.08	1.42 ± 0.16	1.29 ± 0.10	1.88 ± 0.13
C9	1.45 ± 0.08	1.33 ± 0.01	1.49 ± 0.03	1.57 ± 0.08
At 50° flexion				
C1	1.43 ± 0.13	1.94 ± 0.08	1.80 ± 0.14	1.23 ± 0.07
C2	1.43 ± 0.07	2.11 ± 0.06	2.02 ± 0.03	0.85 ± 0.09
C3	1.15 ± 0.11	1.67 ± 0.13	1.47 ± 0.06	1.13 ± 0.10
C4	1.12 ± 0.05	1.80 ± 0.04	1.75 ± 0.07	1.04 ± 0.09
C5	2.43 ± 0.10	2.11 ± 0.07	1.54 ± 0.17	1.82 ± 0.05
C6	1.19 ± 0.01	1.08 ± 0.07	1.93 ± 0.03	1.95 ± 0.06
C7	1.77 ± 0.05	1.52 ± 0.09	1.77 ± 0.08	1.80 ± 0.06
C8	0.97 ± 0.10	1.54 ± 0.10	0.97 ± 0.08	1.26 ± 0.04
C9	1.58 ± 0.12	1.10 ± 0.05	1.58 ± 0.05	1.59 ± 0.03
At 70° flexion				
C1	1.37 ± 0.08	2.03 ± 0.04	2.29 ± 0.20	1.18 ± 0.10
C2	1.74 ± 0.16	1.88 ± 0.21	1.73 ± 0.07	1.18 ± 0.26
C3	1.01 ± 0.10	1.64 ± 0.14	1.54 ± 0.12	1.12 ± 0.07
C4	1.35 ± 0.06	1.71 ± 0.02	1.61 ± 0.09	1.07 ± 0.09
C5	2.53 ± 0.12	2.11 ± 0.06	1.52 ± 0.13	1.33 ± 0.08
C6	1.41 ± 0.14	1.25 ± 0.09	1.77 ± 0.04	1.79 ± 0.03
C7	1.30 ± 0.14	1.52 ± 0.21	2.00 ± 0.04	1.72 ± 0.06
C8	1.49 ± 0.14	1.43 ± 0.07	1.57 ± 0.15	1.16 ± 0.04